Efficient grid treatment of the ionization dynamics of laser-driven H_2^+

Daniel Dundas*
Department of Applied Mathematics and Theoretical Physics, Queen's University Belfast, Belfast BT7 1NN, United Kingdom
(Received 25 June 2001; published 11 January 2002)

We implement a parallel, time-dependent hybrid finite-difference Lagrange mesh code to model the electron dynamics of the fixed-nuclei hydrogen molecular ion subjected to intense ultrashort laser pulses. Ionization rates are calculated and compared with results from a previous finite-difference approach and also with published Floquet results. The sensitivity of the results to the gauge describing the electron-field interaction is studied. Visualizations of the evolving wave packets are also presented in which the formation of a stable bound-state resonance is observed.

DOI: 10.1103/PhysRevA.65.023408 PACS number(s): 33.80.Rv, 02.60.Cb, 02.70.Bf

I. INTRODUCTION

The interaction of a diatomic molecule with an intense, ultrashort laser pulse provides an example of a quantum system driven far from equilibrium. When this interaction occurs, several highly nonlinear phenomena are observed, namely, ionization (multiphoton, tunneling, and above threshold), high-order harmonic generation, dissociation, and Coulomb explosions [1–4]. Whereas the first three processes relate to the electron dynamics, as evidenced by the fact that they are also observed in atomic systems [5], the last two clearly bring the nuclear dynamics into play. Nevertheless, the nuclear dynamics involve a critical interplay with the electron dynamics since the electrons interact directly with the laser field. Hence an accurate description of all the above processes requires a precise description of the electron dynamics [6].

The origin of these nonlinear processes is best studied by considering the simplest diatomic molecules, namely, the one-electron hydrogen molecular ion and the two-electron hydrogen molecule. While both dimers allow study of the dissociation processes, the two-electron hydrogen molecule allows electron correlation effects in the electron dynamics to be explored. Most experimental studies to date have focused on the neutral molecule [1]. This has been due to the relative ease of preparing neutral beams. Indeed, it has only been in the last few years that experimental techniques have advanced to the point where ion beams can be utilized [7,8].

An accurate theoretical description of laser-driven dimers requires the solution of the time-dependent Schrödinger equation (TDSE),

$$H(\mathbf{r},t)\Psi(\mathbf{r},t)=i\hbar\frac{\partial}{\partial t}\Psi(\mathbf{r},t), \tag{1.1}$$

where $H(\mathbf{r},t)$ is the time-dependent Hamiltonian and $\Psi(\mathbf{r},t)$ the wave function. Taking only parallel electronic transitions into account the molecular ion with fixed internuclear spacing interacting with a linearly polarized laser pulse demands the solution of a $(2+1)$-dimensional TDSE while the hydrogen molecule amounts to a $(5+1)$-dimensional problem. These problems are thus comparable with the hydrogen atom and helium atom, respectively, but with the complexity of two centres of nuclear charge. The treatment of multielectron systems in full dimensionality is a formidable task and it is only recently that such calculations for atoms [9–11] have begun to uncover the subtleties in the dynamics induced by the electron-electron interaction. For molecules this has meant that, in contrast with experiment, most serious numerical work is still limited to the molecular ion.

Solution of the TDSE has generally followed two approaches. For the long pulse, low-intensity regime the time-independent Floquet method is applicable and has had much success in treating both the molecular-ion problem through use of an electronic basis of Sturmian functions [12–14], and the molecular problem using an *R*-matrix basis [15,16]. In treating the high-intensity, short-pulse regime used in many present day experiments, direct time-dependent grid approaches are most appropriate [17–23].

The grids used in such time-dependent calculations must give an adequate coverage of configuration space while not using too many points in mapping out less important coordinates. For a linearly polarized laser pulse with the internuclear axis aligned along the polarization axis, cylindrical polar coordinates can be used, the electron position vector being given by

$$\mathbf{r}=\rho\cos(\phi)\mathbf{i}+\rho\sin(\phi)\mathbf{j}+z\mathbf{k}, \tag{1.2}$$

where the axial coordinate (z) is along the polarization direction. The z coordinate is, therefore, predominant since most electron motion will take place along the axis of polarization. The radial coordinate (ρ), while less important, is still required for a proper description of the exchange of angular momentum between the electrons and the field.

The principal grid technique used has been the finite-difference method. Applying this method in cylindrical coordinates leads to problems brought about by enforcing the correct boundary conditions at $\rho=0$. Scaled coordinates have been introduced to alleviate this problem using both a length gauge description of the laser-electron interactions [18,21] and, more recently, an acceleration gauge description [23]. However, the scaled finite-difference matrices in the ρ direction are non-hermitian leading to a nonunitary time evolution. Whilst unitary is recovered in the limit of decreasing

*Electronic address: d.dundas@qub.ac.uk

grid spacing this nevertheless means that more grid points are required to cover an adequate range in configuration space. Although this is not an insurmountable problem for the description of the molecular ion, it poses serious problems in the $(5+1)$-dimensional treatment of the H_2 molecule.

Methods that work well not only for the one-electron hydrogen molecular ion but also for the two-electron molecule must satisfy the following requirements: (1) allow the correct application of the boundary conditions at $\rho=0$; (2) make possible a unitary time-evolution operator; (3) require comparatively few grid points along the ρ direction.

In this paper, we introduce a method that satisfies all the above requirements, namely, a Lagrange mesh treatment of the ρ coordinate together with a finite-difference treatment of the z coordinate. In order to show the power of the method, we limit ourselves to a description of the one-electron molecular ion and make a comparison with other time-dependent and time-independent approaches. The paper is set out as follows. In Sec. II, we establish the Lagrange mesh technique and show how it leads to a set of grid equations. In Sec. III, we describe how the Lagrange mesh can be combined with the finite-difference method in order to describe the molecular ion. The TDSE for the molecular ion is derived and a set of grid equations obtained. Other aspects of the numerical technique are detailed such as time propagation; generation of an initial state; splitting of the wave function to prevent reflections from the edges of the grid; and gauge choice for the electron-laser interaction. Section IV presents various results. In particular, the method is benchmarked against the Floquet method and a previous method using scaled finite differences reported in Ref. [21], hereafter referred to as (**I**). Scientific visualization techniques are then used to analyze the time evolution of the electron dynamics. Finally some conclusions about the strength of the method are drawn. Atomic units are used throughout.

II. LAGRANGE MESH TECHNIQUE

The Lagrange mesh method is a basis-set method founded on Lagrange interpolation and Gaussian quadrature. It is a special case of the discrete variable representation method [24] that has been extensively applied to both time-independent problems [25,26] and time-dependent problems [27–29]. In this section, we give an outline of the method. For a fuller description of the method, the reader is referred to Baye and Heenan [30].

Consider a set of N differentiable functions $f_i(x)$ defined on a domain $a\leqslant x\leqslant b$ with $i=1,2,...,N$. These basis functions satisfy the Lagrange interpolation condition

$$f_i(x_j)=\lambda_i^{-1/2}\delta_{ij}, \tag{2.1}$$

and the Gaussian quadrature

$$\langle f_i|f_j\rangle\equiv\int_a^b f_i^*(x)f_j(x)dx\approx\lambda_i^{1/2}f_i^*(x_j)=\lambda_i^{1/2}f_j(x_i)=\delta_{ij}, \tag{2.2}$$

with mesh points x_i and weights λ_i and lead to a set of grid equations whose grid points are the quadrature pivots.

A. Construction of the Lagrange functions

In order to construct the basis functions, we first consider N differentiable basis functions $\varphi_k(x)$ defined on the domain $a\leqslant x\leqslant b$ with $k=0,1,...,N-1$ and which satisfy the orthonormality conditions

$$\langle\varphi_i|\varphi_j\rangle=\delta_{ij}. \tag{2.3}$$

Then provided

$$\sum_{k=0}^{N-1}\varphi_k^*(x_i)\varphi_k(x_j)=\lambda_i^{-1}\delta_{ij}, \tag{2.4}$$

we can construct

$$f_i(x)=\lambda_i\sum_{k=0}^{N-1}\varphi_k^*(x_i)\varphi_k(x) \tag{2.5}$$

such that

$$\lambda_i=\left[\sum_{k=0}^{N-1}|\varphi_k(x_i)|^2\right]^{-1}, \tag{2.6}$$

satisfying Eqs. (2.1) and (2.2).

B. Obtaining the grid equations

To show how the grid equations are obtained, we apply the method to a one-dimensional (1D), time-dependent problem. Starting from the TDSE

$$H(x,t)\Psi(x,t)=[T+V(x,t)]\Psi(x,t)=i\frac{\partial}{\partial t}\Psi(x,t), \tag{2.7}$$

where T is the kinetic-energy operator $V(x,t)$ a potential and $\Psi(x,t)$ the wave function. We expand the wave function in the Lagrange basis

$$\Psi(x,t)\approx\sum_{i=1}^{N}c_i(t)f_i(x), \tag{2.8}$$

where $c_i(t)$ are expansion coefficients. Clearly

$$c_i(t)=\int_a^b f_i^*(x)\Psi(x,t)dx\approx\lambda_i^{1/2}\Psi(x_i,t). \tag{2.9}$$

Substituting Eq. (2.8) into (2.7), taking the inner product of both sides with an arbitrary basis member $f_j(x)$, using Eq. (2.1) and (2.2) and introducing the linear scaling $y_i=hx_i$ leads to

$$\sum_{j=1}^{N}\left[\frac{1}{h^2}T_{ij}+V(y_i,t)\delta_{ij}-i\frac{\partial}{\partial t}\delta_{ij}\right]\lambda_j^{1/2}\Psi(y_j,t)=0, \tag{2.10}$$

where $T_{ij}=\langle f_i|T|f_j\rangle$. We see that this equation represents a set of linear equations, where we need only to evaluate the potential term and the wave function at the mesh points.

C. Application to the range [0, ∞)

Since we are interested in treating the ρ coordinate with the Lagrange mesh, we must construct a basis defined on the interval $[0, \infty)$. The generalized Laguerre polynomials,

$$L_n^{(\alpha)}(x)=\frac{(\alpha+n)!}{\alpha!n!}\,{}_1F_1(-n;\alpha+1;x), \tag{2.11}$$

defined over the interval $[0, \infty)$ and associated with the weight function $x^\alpha e^{-x}$, fit this criterion perfectly. Defining N orthonormal functions $\varphi_n(x)$ with $n=0,1,2,...,N-1$ as

$$\varphi_n(x)=\frac{\Gamma(\alpha+n+1)}{n!}x^{\alpha/2}e^{-x/2}L_n^{(\alpha)}(x), \tag{2.12}$$

the corresponding Lagrange functions are given by

$$f_i(x)=\lambda_i^{-1/2}\left(\frac{1}{\varphi_N'(x_i)}\right)\frac{\varphi_N(x)}{x-x_i}, \tag{2.13}$$

where x_i are the zeros of $L_N^{(\alpha)}(x)$ and

$$\lambda_i=\frac{1}{x_i\varphi_N'(x_i)^2}. \tag{2.14}$$

The generalized Laguerre polynomials are associated with the kinetic-energy operator

$$T=\frac{1}{2\mu}\left(-\frac{\partial^2}{\partial x^2}+\frac{\alpha(\alpha-2)}{4x^2}\right), \tag{2.15}$$

where μ is the reduced mass of the electron. Baye and Heenen [30] showed that the matrix elements T_{ij} are given by

$$T_{ij}=\frac{1}{2\mu}\times\begin{cases}\dfrac{(\alpha+1)^2}{4x_i^2}+S_{ii}, & i=j\\[2ex] (-1)^{i-j}\left[\dfrac{\alpha+1}{2\sqrt{x_ix_j}}\left(\dfrac{1}{x_i}+\dfrac{1}{x_j}\right)+S_{ij}\right], & i\neq j,\end{cases} \tag{2.16}$$

where

$$S_{ij}=\sqrt{x_ix_j}\sum_{k\neq i,j}\frac{1}{x_k(x_k-x_i)(x_k-x_j)}. \tag{2.17}$$

III. APPLICATION TO H_2^+

Turning our attention to the molecular ion, it is now shown how the Lagrange mesh approach can be combined with finite differences to solve the TDSE. For Σ-symmetry, the azimuthal (ϕ) dependence does not arise and the Hamiltonian has the form

$$H=-\frac{1}{2\mu}\left\{\frac{\partial^2}{\partial z^2}+\frac{1}{\rho}\frac{\partial}{\partial\rho}\rho\frac{\partial}{\partial\rho}\right\}+V(\rho,z,R)+U(z,t), \tag{3.1}$$

where $V(\rho,z,R)$ represents the Coulomb interactions

$$V(\rho,z,R)=-\frac{Z_1}{[\rho^2+(z-\frac{1}{2}R)^2]^{1/2}}-\frac{Z_2}{[\rho^2+(z+\frac{1}{2}R)^2]^{1/2}}+\frac{Z_1Z_2}{R}, \tag{3.2}$$

R being the internuclear distance and Z_1 and Z_2 being the nuclear charges; and $U(z,t)$ represents the interaction between the electron and the laser field. In most of the results presented in this paper the length gauge description of the electron-field interaction is used, given by

$$U_L(z,t)=zE(t), \tag{3.3}$$

where $E(t)$ is the electric-field strength in the dipole approximation given by

$$E(t)=E_0q(t)\cos\omega t, \tag{3.4}$$

for a field with frequency ω and is related to the *peak* laser intensity I_0 by

$$E_0=\left(\frac{4\pi I_0}{c}\right)^{1/2}. \tag{3.5}$$

Since the laser field is pulsed we include the pulse envelope $q(t)$, which consists of a smooth ramp on from zero to one over a duration t_1. The field amplitude is then held constant from a time t_1 to a time t_2 after which it is ramped off to zero at a time t_3, the ramp off time being equal to the ramp on time ($t_1=t_3-t_2$). Thus,

$$q(t)=\begin{cases}\frac{1}{2}\left[1-\cos\left(\dfrac{\pi t}{t_1}\right)\right], & 0\leqslant t\leqslant t_1\\[2ex] 1, & t_1\leqslant t\leqslant t_2\\[2ex] \frac{1}{2}\left[1-\cos\left(\dfrac{\pi(t-t_2+t_1)}{t_1}\right)\right], & t_2\leqslant t\leqslant t_3\\[2ex] 0 & \text{otherwise.}\end{cases} \tag{3.6}$$

A velocity gauge description of the electron-field interaction can also be used in which

$$U_V(z,t)=-\frac{i}{c}A(t)\frac{\partial}{\partial z}, \tag{3.7}$$

where c is the speed of light and $A(t)$ is the vector potential of the laser field that is related to the electric-field strength via

$$E(t)=-\frac{1}{c}\frac{\partial A(t)}{\partial t}, \tag{3.8}$$

One can remove the first-order derivative in Eq. (3.1) by the change of dependent variable

$$\Psi(\rho,z,t)=\rho^{-1/2}\psi(\rho,z,t), \tag{3.9}$$

such that

$$i\frac{\partial}{\partial t}\psi(\rho,z,t)=\left[-\frac{1}{2\mu}\frac{\partial^2}{\partial z^2}+D_\rho+V(\rho,z,R)+U(z,t)\right]\psi(\rho,z,t), \tag{3.10}$$

where

$$D_\rho=\frac{1}{2\mu}\left(-\frac{\partial^2}{\partial\rho^2}-\frac{1}{4\rho^2}\right). \tag{3.11}$$

In this case wave function normalization requires

$$\int_0^\infty d\rho\int_{-\infty}^{+\infty}dz|\psi(\rho,z,t)|^2=1. \tag{3.12}$$

We then construct a 2D grid in the ρ and z coordinates and discretize the wave function on this grid.

A. Lagrange mesh treatment of the ρ coordinate

The Lagrange mesh method is now applied to the treatment of the ρ coordinate by expanding the wave function as in Eq. (2.8), namely,

$$\psi(\rho,z,t)=\sum_{i=1}^{N}\lambda_i^{1/2}\psi(\rho_i,z,t)f_i(\rho). \tag{3.13}$$

This allows us to obtain the TDSE

$$\sum_{j=1}^{N}\left[-\frac{1}{2\mu}\frac{\partial^2}{\partial z^2}\delta_{ij}+\frac{1}{h^2}D_{ij}+V(\overline{\rho_i},z,R)\delta_{ij}+U(z,t)\delta_{ij}-i\frac{\partial}{\partial t}\delta_{ij}\right]\lambda_j^{1/2}\psi(\overline{\rho_j},z,t)=0, \tag{3.14}$$

where $D_{ij}=\langle f_i|D_\rho|f_j\rangle$ and we employ the linear scaling $\overline{\rho_i}=h\rho_i$. Furthermore, we see that Eq. (3.11) corresponds to Eq. (2.15) when $\alpha=1$ and so D_{ij} is given by Eq. (2.16).

Convergence studies have shown that for all the results presented in this paper $N=30$ basis functions are sufficient. It was also found that while ionization rates are not sensitive to the scaling parameter h, converged harmonic generation spectra were only obtained whenever the scaling parameter was reduced to $h=0.4$. This results in a mesh having an extent $0\leqslant\overline{\rho}\leqslant 42$.

B. Finite difference treatment of z

As in (**I**) the z coordinate is treated using finite differences. The kinetic-energy term is approximated by the five-point central difference formula

$$f''(z)=\frac{1}{(\delta z)^2}\left[-\tfrac{1}{12}f(z-2\delta z)+\tfrac{16}{12}f(z-\delta z)-\tfrac{30}{12}f(z)+\tfrac{16}{12}f(z+\delta z)-\tfrac{1}{12}f(z+2\delta z)\right], \tag{3.15}$$

and the first derivative required for the calculation of $U_V(z,t)$ is approximated by

$$f'(z)=\frac{1}{(\delta z)}\left[\tfrac{1}{12}f(z-2\delta z)-\tfrac{8}{12}f(z-\delta z)+\tfrac{8}{12}f(z+\delta z)-\tfrac{1}{12}f(z+2\delta z)\right]. \tag{3.16}$$

The finite-difference approach allows us to parallelize our computer code efficiently. The z coordinate grid is distributed across processors while the ρ mesh is handled entirely on each processor. In order to handle the electron quiver motion in intense fields a large number of z grid points must be used. Distributing the z coordinate across processors allows us to scale the size of the problem easily to describe intense fields. The sparse nature of the finite-difference matrices compared to the Lagrange mesh method means that communications between processors is kept to a minimum. Indeed each processor must communicate with a maximum of four neighboring processors, depending on how many z points are stored per processor. We have already dealt with convergence studies against δz in (**I**) and so will not detail this again. Briefly, we find that converged results are obtained for a grid spacing of $\delta z=0.2$.

C. Arnoldi time propagator

Given a wave function $\psi(t)$ at a time t the wave function at a later time $t+\delta t$ is obtained by applying the unitary time-evolution operator $U(t+\delta t,t)$, namely,

$$\psi(t+\delta t)=U(t+\delta t,t)\psi(t)\approx e^{-iH(t)\delta t}\psi(t). \tag{3.17}$$

In (**I**) the ρ coordinate was treated using finite differences in scaled coordinates. The finite-difference matrices were non-Hermitian and so the time-evolution operator was nonunitary. In that case $U(t+\delta t,t)$ was approximated by its nth order Taylor-series expansion

$$U(t+\delta t,t)=\sum_{k=0}^{n}\frac{(-i\delta t)^k}{k!}H^k(t). \tag{3.18}$$

In the present work the matrix elements of D_ρ in the Lagrange basis are hermitian leading to a unitary time-evolution operator. We, therefore, wish to use an accurate, high-order unitary time-evolution operator and hence choose the nth-order Arnoldi propagator [31]. The Arnoldi propagator is an explicit propagator that involves successive operations of the Hamiltonian upon the wave function in much the same way as the Taylor-series propagator. Using the Arnoldi algorithm [32], we construct an orthonormal set of vectors, $[q_0,q_1,q_2,\ldots,q_n]$, which span the Krylov subspace

$$K_n(H,\psi) \equiv \text{span}\{\psi, H\psi, H^2\psi, \ldots, H^n\psi\}. \quad (3.19)$$

The orthonormal set is formed using Gram-Schmidt orthogonalization. The process may be represented schematically as follows:

(1) Construct the first orthonormal unit vector as

$$q_0 = \psi/|\psi|^{1/2}.$$

(2) For $j=0,1,2,...,n$

Compute the next vector spanning the subspace, $v = Hq_j$.

For $i=0,1,2,...,j$

Compute the projection of v onto those q_i already calculated, i.e., $h_{ij} = q_i^\dagger v$.

Subtract the projection of those q_i already calculated so that v will be orthogonal to q_i, i.e., $v = v - h_{ij} q_i$.

Compute $h_{j+1,j} = |v|^{1/2}$ and the unit vector $q_{j+1} = v/h_{j+1,j}$.

next i

next j

Letting h denote the $(n+1)\times(n+1)$ upper-Hessenberg matrix formed by the coefficients h_{ij}, we obtain the matrix equation

$$h = Q^\dagger H Q, \quad (3.20)$$

where Q is a matrix formed from the N column vectors $[q_0, q_1, q_2, \ldots, q_n]$ and so h is the Krylov subspace Hamiltonian that is calculated simultaneously with Q. $\tilde{H} = Q^\dagger h Q$ can be used as a replacement to H in a wide variety of applications. In particular, the time-evolution operator can be written as

$$\tilde{U}(t+\delta t, t) = e^{-i\tilde{H}\delta t} = Q e^{-ih\delta t} Q^\dagger. \quad (3.21)$$

Now h is typically a tridiagonal matrix and so $e^{-ih\delta t}$ can be inexpensively exponentiated through the direct diagonalization of h. $\tilde{U}(t)$ may thus be viewed as a unitary propagator that is correct to order n in δt. In the present work converged time propagation is obtained using a sixth-order Arnoldi propagator using a time step, $\delta t = 0.01$.

D. Obtaining the initial state

In (**I**) it was shown how the ground state of the hydrogen molecular ion could be obtained by propagating the wave function in imaginary time, i.e., by the replacement $\tau = it$. With this replacement the evolution operator, Eq. (3.21), becomes $\tilde{U}(t) = Q e^{-h\delta\tau} Q^\dagger$. This has the effect of turning the TDSE from a wave equation into a diffusion equation, in which the eigenvectors decay at rates proportional to their energies. The effect is that only the lowest eigenvector survives (the ground state). This process of excited state decay lasts no longer than 50 a.u.

Lanczos showed that the eigendecomposition of h can be used as a first step in an iterative scheme to calculate the eigenvalues of H. This approach proves attractive in obtaining the ground state of the molecular ion instead of using a diffusion equation since the ground state is obtained more rapidly. Indeed we find that only one hundred iterations are required to obtain convergence. This corresponds to 100 applications of the propagator upon the wave function compared to 5000 applications of the propagator upon the wave function using the diffusion equation with a time spacing $\delta t = 0.01$.

E. Wave function splitting

Wave packets that reach the edge of the grid can be reflected from the boundary causing spurious effects in both harmonic spectra and ionization rates. We eliminate these reflections by a splitting technique akin to an absorbing boundary that partitions the wave function into two parts, one near, and the other far from the nuclei where the Coulomb potential is negligible. This technique was introduced by Heather and Metiu [33] and has been applied to laser-atom interactions [31], fixed nuclei H_2^+ [21], and vibrating nuclei H_2^+ [34]. Recently the technique has been expanded by Bandrauk and co-workers in its application to a 1D model of vibrating nuclei H_2^+ by projecting onto asymptotic Volkov states allowing, amongst other things, complete calculations of Coulomb explosion spectra for the residual protons [35,36]. The splitting is implemented by a mask function M, which equals unity near the nuclei and goes asymptotically to zero very gradually. Using this mask function the wave function is split into two parts

$$\psi = M\psi + (1-M)\psi. \quad (3.22)$$

The residual part, $(1-M)\psi$, can be propagated independently in the limit in which the Coulomb potential is negligible over the region in which $M<1$. The design and optimization of the mask function requires considerable care, and extensive numerical simulations must be performed to characterize the optimal shape [31].

While the use of such absorbing boundaries is well documented in finite difference methods, their use with Lagrange meshes has not been described in great detail. For instance, recently Sakimoto [29] used a Laguerre-Lagrange mesh in a time-dependent treatment of excitation and ionization in $\bar{p}+H$ collisions. It was noted that because the Laguerre polynomials spanned the range $[0,\infty)$ reflections would not occur and, therefore, no form of absorption was necessary. This, however, will only be the case if an infinite number of mesh points are used in the calculation. In all calculations the number of mesh points is truncated at some finite value yielding a numerical grid with finite extent. Hence reflections will occur if no form of wave function splitting is used. As in (**I**), the mask function is broken into a $\bar{\rho}$-dependent part $M_{\bar{\rho}}(\bar{\rho})$ and a z-dependent part $M_z(z)$ given, respectively, by

$$M_{\bar{\rho}}(\bar{\rho}) = \exp\left[-4\left(\frac{\bar{\rho}-\alpha\bar{\rho}_{\max}}{\bar{\rho}_{\max}\sigma}\right)^2\right]$$

$$\text{if } \bar{\rho} > \alpha\bar{\rho}_{\max}, \quad (3.23)$$

where $\bar{\rho}_{\max}$ is the maximum value of $\bar{\rho}$ and

$$M_z(z)=\exp\left[-4\left(\frac{|z|-\alpha Z_{\max}}{Z_{\max}\sigma}\right)^2\right]$$

$$\text{if } |z|>\alpha Z_{\max}, \tag{3.24}$$

where $Z_{\max}$ is the maximum value of z and $M_{\bar{\rho}}(\bar{\rho})=M_z(z)=1$ otherwise. The wave function is thus split according to

$$\psi(\bar{\rho},z,t)=M_z M_{\bar{\rho}}\psi(\bar{\rho},z,t)+(1-M_z M_{\bar{\rho}})\psi(\bar{\rho},z,t), \tag{3.25}$$

where $\psi_s(\bar{\rho},z,t)=M_z(z)M_{\bar{\rho}}(\bar{\rho})\psi(\bar{\rho},z,t)$ is the split wave function. The optimal values of α and σ were determined empirically to be $\alpha\approx 0.3$ and $\sigma\approx 5$. We note that the mask function does not have to equal zero at the boundary. The only requirement is that ψ smoothly approaches zero at the edges of the integration volume.

IV. RESULTS

We now present results using this method making a comparison with the scaled finite-difference treatment of the ρ coordinate and with Floquet results. Scientific visualization techniques are then used to analyze the time evolution of the electron dynamics in the presence of a resonance. A grid having extent $-50\leqslant z\leqslant 50$ and $0\leqslant\bar{\rho}\leqslant 42$ is used in all calculations.

A. Calculation of the grid energy spectrum

We have already discussed how the field-free ground electronic state of the grid can be obtained by either propagation of a trial wave function in imaginary time or by a Lanzcos eigendecomposition. However, neither of these methods tell us how accurately the excited states of the molecular ion are represented on the grid (the Lanzcos algorithm that is currently implemented in our code only gives information on the lowest eigenvalue).

In order to calculate the excited-state energies, we can use a time autocorrelation technique [37]. This consists of calculating the time autocorrelation function

$$C(t)=\int \psi_t^*(\mathbf{r},t)\psi_t(\mathbf{r},0)d\mathbf{r}, \tag{4.1}$$

where

$$H_{\rm el}\psi_t(\mathbf{r},t)=i\frac{\partial}{\partial t}\psi_t(\mathbf{r},t), \tag{4.2}$$

by propagating a trial function $\psi_t(0)$, in real time in the absence of the laser field, $H_{\rm el}$ being the field-free electronic Hamiltonian. The spectral density of this, obtained by taking the square of its Fourier transform

$$|C(\omega)|^2=\left|\int_0^\infty C(t)e^{i\omega t}dt\right|^2, \tag{4.3}$$

gives us the energies of states supported by the grid. The trial function includes even and odd parities. In this work, we choose

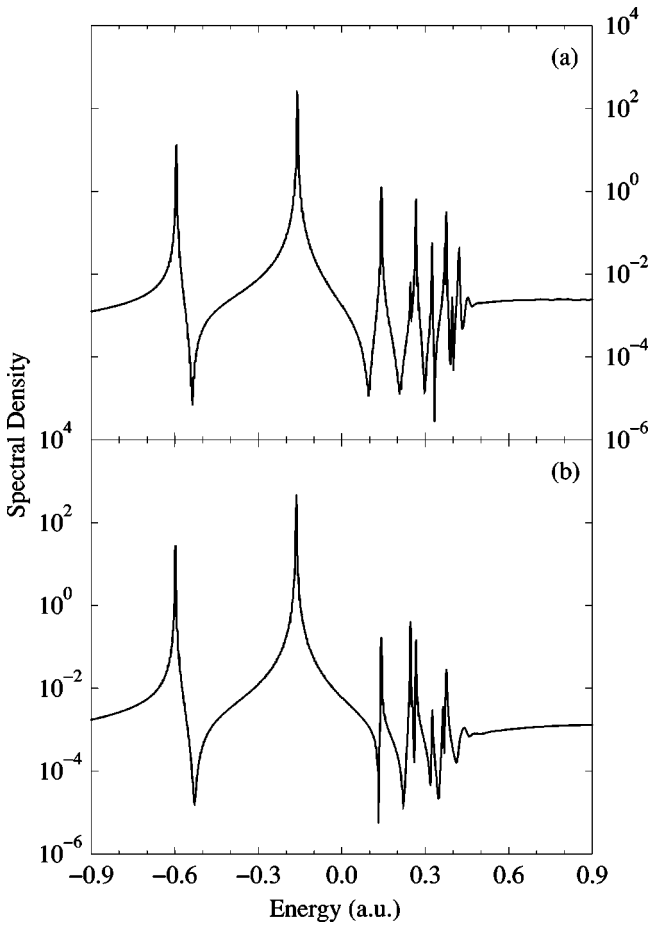

FIG. 1. Spectral density $|C(\omega)|^2$ at $R=2$ using (a) the Lagrange mesh model and (b) the finite difference model. In both cases a finite difference grid in z is used.

$$\psi_t(\mathbf{r},0)=\psi_g(1+z+z^2)(1+\bar{\rho}+\bar{\rho}^2)e^{-z^2}, \tag{4.4}$$

where ψ_g is the analytic form of the $\Sigma_g 1s$ variational ground state, namely, [38]

$$\psi_g=[e^{-\alpha(r_a+r_b)}], \tag{4.5}$$

with $\alpha=1.24$ and

$$r_{a,b}=[\bar{\rho}^2+(z\pm R/2)^2]^{1/2}. \tag{4.6}$$

Figure 1 presents the electronic energy spectrum of the grid for a fixed nuclei calculation at $R=2$ using both the Lagrange mesh treatment of ρ [Fig. 1(a)] and the finite-difference treatment [Fig. 1(b)]. A range of states are present up to the ionization limit at 0.5. Table I presents a comparison with results given by Sharp [39]. The two sets of results are in quite good agreement with the Sharp data although there are slight inaccuracies in certain excited-state energies that is to be expected due to the discretizion and finite extent of the grids affecting such cases. On the whole the energies using the Lagrange mesh approach are more accurate than those from the finite-difference method for the parameters chosen. The results from both methods, however, present

TABLE I. Energies of electronic states using the finite difference ($\delta z=0.2, \delta\rho=0.15$) and Lagrange mesh ($\delta z=0.2, N=30$) calculations of fixed nuclei H_2^+ at $R=2$ compared with energies given by Sharp [39].

Possible states Sharp data	Peaks in graph Finite difference Lagrange mesh		
State	Energy (a.u.)	Energy (a.u.)	
$\Sigma_g 1s$	−0.602	−0.599	−0.599
$\Sigma_u 1s$	−0.167	−0.163	−0.161
$\Sigma_g 2s$	0.139	0.141	0.141
$\Sigma_u 2s$	0.245	0.247	0.247
$\Sigma_g 2p$	0.264	0.266	0.264
$\Sigma_g 3s$	0.315	0.326	0.323
$\Sigma_g 3p$	0.366	0.364	
$\Sigma_u 2p$	0.373	0.376	0.372
$\Sigma_g 4s$	0.394		0.394
$\Sigma_u 4s$	0.414		↑
$\Sigma_u 3p$	0.416		
$\Sigma_g 3d$	0.417		0.418
$\Sigma_g 4p$	0.417		↓
$\Sigma_u 3d$	0.441	0.440	
$\Sigma_u 4p$	0.444		↑
$\Sigma_g 4d$	0.444		
$\Sigma_u 4d$	0.459		0.449
$\Sigma_g 4f$	0.459		↓
$\Sigma_u 4f$	0.468		

convincing evidence that grid methods give an accurate representation of the electronic structure.

B. Gauge dependence of ionization rate

In principle, the two approaches outlined for describing the electron-field interactions are equivalent since the length gauge description is related to the velocity gauge description through the unitary transformation

$$\Psi_V(\mathbf{r},t)=\exp\left[\frac{i}{c}\mathbf{r}\mathbf{A}(t)\right]\Psi_L(\mathbf{r},t). \tag{4.7}$$

In practice the length and velocity descriptions do not necessarily agree since the wave function is approximated. Gauge effects have already been well documented in atomic systems [40,41]. However, time-dependent molecular approaches generally use a length gauge solution while other approaches such as the time-independent Floquet results presented in this paper for comparison have used a velocity gauge description. Whilst gauge comparison have been made using the Floquet results, few time-dependent approaches make such a comparison. For instance, Bandrauk and coworkers have recently made a detailed comparison of length and acceleration gauge descriptions using a scaled finite-difference technique [23]. In the following, we make a comparison between the length and velocity gauges. Since the purpose of this paper is to present an efficient method that can be used to treat H_2 we will not deal with the acceleration gauge since it would involve the calculation of large time-dependent Coulomb potential terms. In Fig. 2 we present the length and velocity gauge comparison of the population within the grid for fixed nuclei H_2^+ at an internuclear separation of $R=8$ for a laser pulse with a wavelength of 248 nm and a peak intensity of 1.0×10^{14} W cm^{-2}. In this case, we see that the results are gauge independent. Indeed, we have checked that other results presented throughout this paper are also gauge independent.

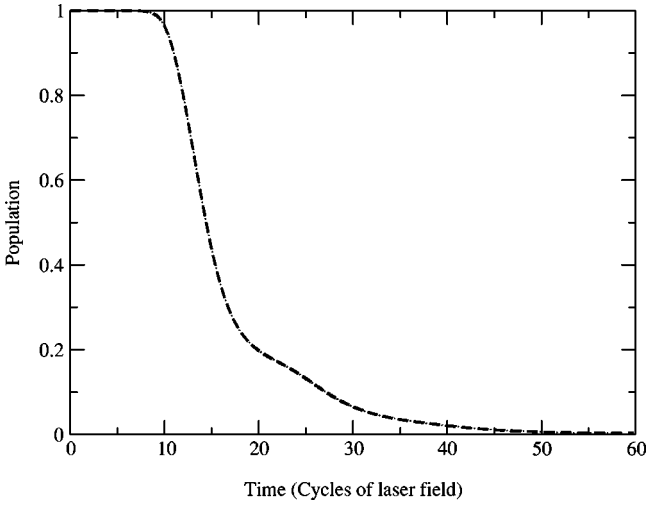

FIG. 2. Length (----) and velocity (·····) gauge comparison of the population within the grid for fixed nuclei H_2^+ at an internuclear separation of $R=8$ for a laser pulse having a wavelength of $\lambda=248$ nm and a peak intensity of $I_0=1.0\times10^{14}$ W cm^{-2}.

C. Floquet comparison

In Fig. 3, we compare our time-dependent results for H_2^+ at $R=2$ using the Lagrange mesh and the finite-difference methods with results from the Floquet method of Madsen and Plummer [14]. In our time-dependent calculations, a

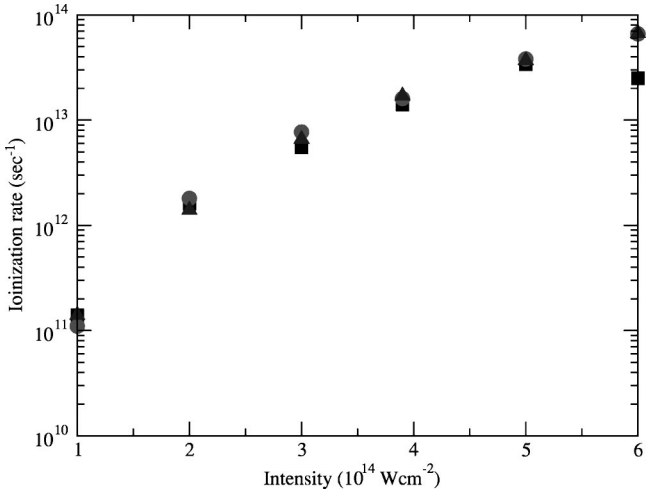

FIG. 3. Comparison of Lagrange mesh (▲) ionization rates at $R=2$ for a wavelength of $\lambda=228$ nm with full finite difference (○) results and Floquet (■) calculations [14].

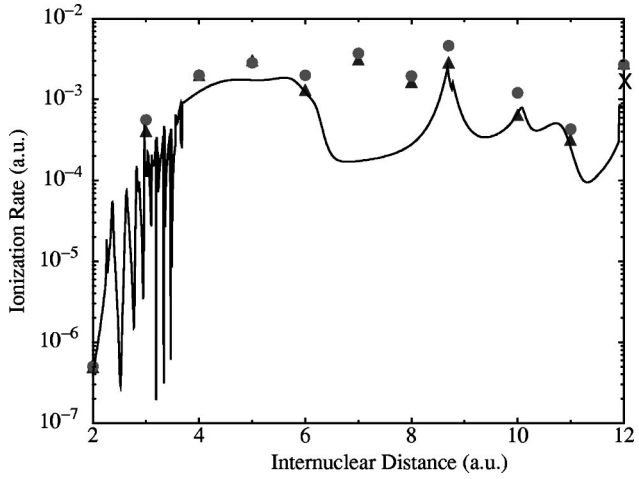

FIG. 4. Comparison of the Lagrange mesh results (▲) for the ionization rate as a function of internuclear separation for a laser pulse of wavelength $\lambda = 248$ nm and peak intensity $I_0 = 1.0 \times 10^{14}$ W cm^{-2} with the results of Madsen and Plummer [14] (——) and with the finite difference method [21] (●). The × at $R = 12$ represents the separated atom ionization rate of 1.44×10^{-3}.

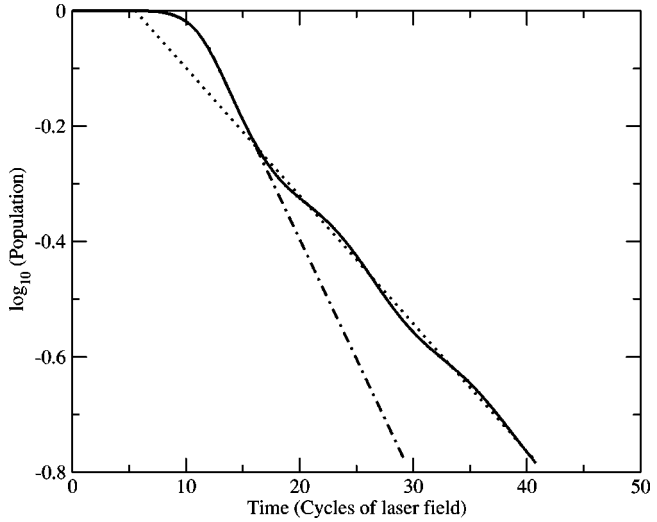

FIG. 5. Logarithm of the electronic population within the grid (——) at $R = 10$ for a wavelength of $\lambda = 248$ nm using and a peak intensity of $I_0 = 1.0 \times 10^{14}$ W cm^{-2}. Two distinct rates are present that are highlighted by the extrapolated lines, namely, initial population of a bound resonant state (—·—) followed by its subsequent decay (·····).

pulse that ramps up over 6 optical cycles, remains constant in intensity for a further 8 cycles and then ramps off over 6 further cycles is used. Results from both approaches show good agreement with Floquet theory. The general trend as a function of intensity is very well reproduced and the absolute ionization rates are in good agreement except at the highest intensity where the Floquet results show a decrease in ionization rate. This drop in rate is attributed to channel closing—that is the Stark shifting of the ground state with respect to the continuum being sufficient at this intensity for seven photons to be required for ionization instead of six. In this regime of frequency and intensity (Keldysh parameter $\gamma \approx 2$) the process is dominated by resonant enhancement. We have investigated the sensitivity of both the finite difference and Lagrange mesh results with grid spacings, grid sizes, and pulse characteristics and found that the results are well converged. Therefore, we attribute the small discrepancy to the slight inaccuracy in the excited state spectrum.

In Fig. 4, we present a comparison of the ionization rates as a function of internuclear separation for a laser pulse of wavelength 248 nm and peak intensity $I_0 = 1.0 \times 10^{14}$ W cm^{-2} with the results of Madsen and Plummer [14] and with the finite-difference method. The Keldysh parameter for these conditions varies between $\gamma \approx 5$ for $R = 2$ and $\gamma \approx 3$ for large R and this defines the process as multiphoton rather than tunneling ionization. Very good agreement between both time-dependent methods is observed for all internuclear distances. Very good agreement with the Floquet results is also found at small internuclear distances at which the ground electronic state is an isolated resonance of the system requiring six photons to reach the ionization threshold, and at larger internuclear distances where the process requires only four photons to achieve ionization. Poor agreement with the Floquet results is observed around intermediate internuclear distances ($6 < R < 9$). The Floquet ionization rates refer to a particular dressed state formed from the Σ_g ground state. However, around intermediate values of R the ground-state ionization rate is difficult to define. As a result of crossings with excited states and Rydberg series resonances the ground state becomes mixed (dressed) with other states. Both wave packet calculations indicate the nonadiabatic following that arises during the pulse rise and indicates the difficulty in comparing with Floquet theory for interfering resonance states. Our results as $R \to \infty$ converge to a separated atom ionization rate of 1.44×10^{-3}, which is marked with a cross on the figure at $R = 12$. This gives excellent agreement with the atomic hydrogen ionization rate of 1.35×10^{-3} calculated by an independent atomic wave packet code utilizing a mixed finite-difference basis-set method [42].

In obtaining these results we found that the use of a 20-cycle laser pulse having a 4 cycle ramp on and a 4 cycle ramp off gave fully converged results except at $R = 8.7$ and $R = 10$. From the figure, we see that the Floquet rate is peaked around these values that suggests the presence of an intermediate resonance state. We find that using a 60 cycle laser pulse having a 10 cycle ramp on and a 10 cycle ramp off reproduces the Floquet rate. The reason for this is obvious from Fig. 5. In this figure, we plot the logarithm of the population within the grid as a function of time at an internuclear separation of $R = 10$. In a nonresonant process, we would expect that after the ramp on period this would decay as a straight line of constant slope. However, we see that two separate rates are present. Firstly, there is a large population decrease from 10–15 cycles after which the rate changes to a lower value with a sinusoidal component superimposed. This implies that an intermediate bound-state resonance is quickly populated at the start of the pulse after which it begins to decay. The sinusoidal component superimposed is due to

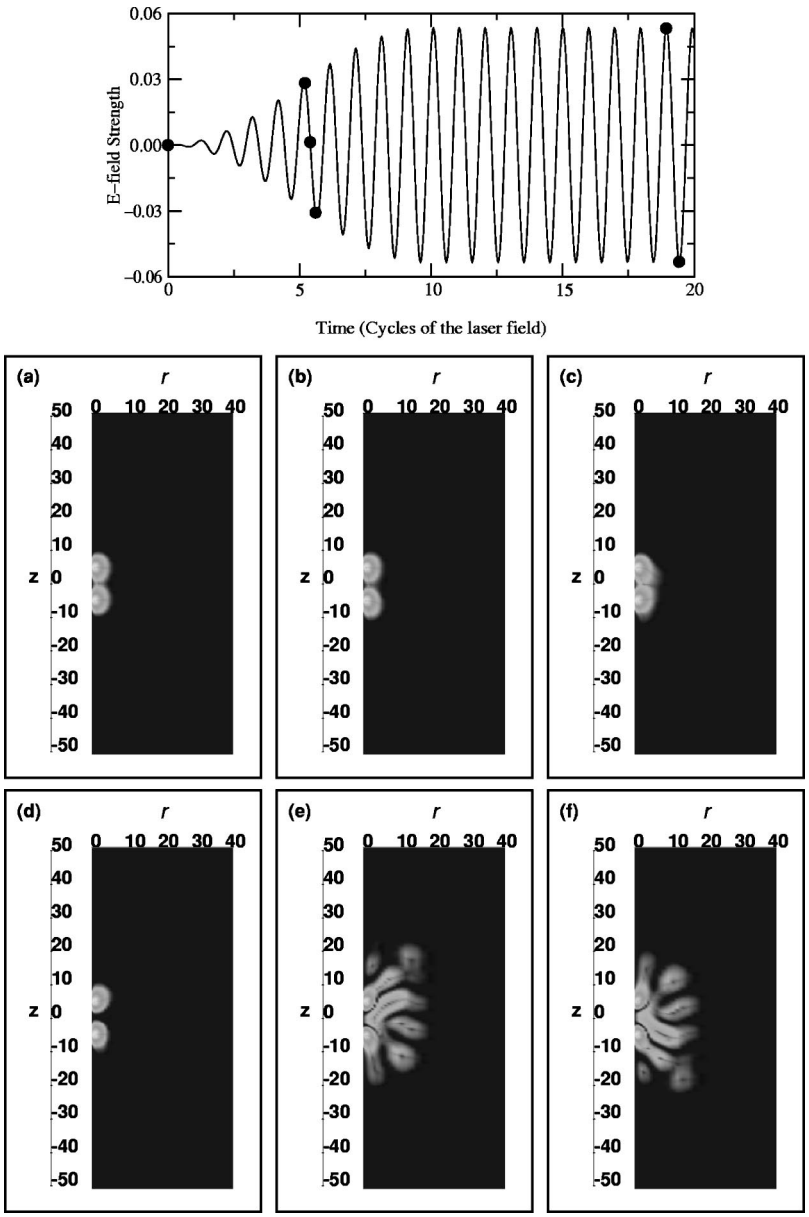

FIG. 6. $\overline{\rho}-z$ plots of the electron probability density $P(\overline{\rho},z,t)$ at $R=10$ for a 60-cycles laser pulse having wavelength $\lambda=248$ nm that ramps up over 10 cycles to a peak intensity of $I_0=1.0\times10^{14}\,\mathrm{W\,cm^{-2}}$. The picture at the top shows a profile of the laser pulse with the circles corresponding (from left to right) to the location of frames (a)–(f). Only 20 cycles of the pulse are shown here for clarity.

Rabi oscillations with the ground state. Such an effect has already been observed in atomic helium through a comparison of the *R*-matrix Floquet method and the direct solution of the TDSE [43].

D. Visualization of the electronic wave packet at large internuclear spacing

Our time-dependent calculations provides us with the complete electronic wave function at each time step in the calculation. Scientific visualization techniques enable us to visualize the electron probability density

$$P(\overline{\rho},z,t)=|\psi(\overline{\rho},z,t)|^2, \tag{4.8}$$

and thus obtain spatial information about the electron dynamics. In (**I**) we presented such a visualization for fixed nuclei H_2^+ at $R=2$ in a $\lambda=248$-nm laser pulse of peak intensity $I_0=6\times10^{14}\,\mathrm{W\,cm^{-2}}$ using the full finite-difference approach. In that case tunneling ionization was dominant and indeed the effects of electron rescattering from the nuclei were observed.

In the ionization results we presented in Fig. 5, we noted a change in ionization rate that was attributed to a bound state becoming resonantly populated followed by its decay. In Fig. 6, $\overline{\rho}$-z plots of the electron probability density for this case are presented at various times during the first 20 cycles of the pulse. The plots show the multiphoton nature of the electron response, especially in frames Figs. 6(a)–(c) where we do not observe any distortion along the z coordinate in antiphase with the field followed by rescattering that we associate with tunnelling ionization [21]. Instead we see that the electric field does cause a different type of distortion, namely, an oscillation whereby electron density is expelled from the region between the two nuclei whenever the field passes through a maxima. Figures 6(e) and 6(f) present plots for two instants at which the decay of the resonant bound

state is observed. The electron wave packet has a well-defined stable structure consisting of six lobes that oscillate in phase with the field. This is the electron distribution of the resonant state. An animation of this electronic density is available in MPEG format from www.am.qub.ac.uk/mecpc/multi1_results.html.

V. CONCLUSIONS

The problem under consideration is one of fundamental importance to femtosecond chemistry through acting as a precursor to the description of more complex molecular systems. In particular, it acts as a stepping stone towards the hydrogen molecule that is widely studied in experiment and acts as the simplest molecular system in which the interplay between electron correlation and dissociation dynamics can be studied. The method that has been presented in this paper represents a general approach for the solution of the hydrogen molecular ion that can readily be scaled to treat the more complex hydrogen molecular problem using present day high-end computational resources. This will be the subject of further publications [44]. The method has shown itself not only to be efficient in the treatment of this problem but also accurate. We note here that the method presents no difficulties in reducing the uncertainty of our solutions, which can be achieved by reducing the grid separations and increasing the grid size.

ACKNOWLEDGMENTS

I would like to thank Ken Taylor, Jim-McCann, and Karen Meharg for helpful discussions during the preparation of this paper. I would also like to thank Jonathan Parker for his help in explaining the intricacies of implementing the Arnoldi propagator. The work reported in this paper is supported in part by the U.K. Engineering and Physical Sciences Research Council by provision of financial support for D.D. as well as resources used at Computer Services for Academic Research, University of Manchester.

[1] K. Codling and L. J. Frasinski, J. Phys. B **26**, 783 (1993).
[2] J. H. Sanderson, R. V. Thomas, W. A. Bryan, W. R. Newell, A. J. Langley, and P. F. Taday, J. Phys. B **31**, L599 (1998).
[3] A. Giusti-Suzor, F. H. Mies, L. F. DiMauro, E. Charron, and B. Yang, J. Phys. B **28**, 309 (1995).
[4] J. F. McCann and J. H. Posthumus, Philos. Trans. R. Soc. London, Ser. A **357**, 1309 (1999).
[5] A. L'Huillier, L. Lompré, G. Mainfray, and C. Manus, in *Atoms in Intense Laser Fields*, edited by M. Gavrila (Academic, Boston, 1992), pp. 139–202.
[6] *Molecules & Clusters in Intense Laser Fields*, edited by J. Posthumus (Cambridge University Press, Cambridge, 2001).
[7] I. D. Williams, P. McKenna, B. Srigengan, I. M. G. Johnston, W. A. Bryan, J. H. Sanderson, A. El-Zein, T. R. J. Goodworth, W. R. Newell, P. F. Taday, and A. J. Langley, J. Phys. B **33**, 2743 (2000).
[8] K. Sändig, H. Figger, and T. W. Hänsch, Phys. Rev. Lett. **85**, 4876 (2000).
[9] K. T. Taylor and D. Dundas, Philos. Trans. R. Soc. London, Ser. A **357**, 1331 (1999).
[10] J. S. Parker, L. R. Moore, D. Dundas, and K. T. Taylor, J. Phys. B **33**, L691 (2000).
[11] J. S. Parker, L. R. Moore, K. J. Meharg, D. Dundas, and K. T. Taylor, J. Phys. B **34**, L69 (2001).
[12] M. Plummer, J. F. McCann, and L. B. Madsen, Comput. Phys. Commun. **114**, 94 (1998).
[13] L. B. Madsen, M. Plummer, and J. F. McCann, Phys. Rev. A **58**, 456 (1998).
[14] L. B. Madsen and M. Plummer, J. Phys. B **31**, 87 (1998).
[15] P. G. Burke, J. Colgan, D. H. Glass, and K. Higgins, J. Phys. B **33**, 143 (2000).
[16] J. Colgan, D. H. Glass, K. Higgins, and P. G. Burke, J. Phys. B **34**, 2089 (2001).
[17] S. Chelkowski, S. Zuo, and A. D. Bandrauk, Phys. Rev. A **46**, R5342 (1992).
[18] H. Kono, A. Kita, Y. Ohtsuki, and Y. Fujimura, J. Comput. Phys. **130**, 148 (1997).
[19] I. Kawata, H. Kono, and Y. Fujimura, Chem. Phys. Lett. **289**, 546 (1998).
[20] I. Kawata, H. Kono, and Y. Fujimura, J. Chem. Phys. **110**, 11 152 (1999).
[21] D. Dundas, J. F. McCann, J. S. Parker, and K. T. Taylor, J. Phys. B **33**, 3261 (2000).
[22] D. Dundas, J. F. McCann, and K. T. Taylor, *Super-Intense Laser-Atom Physics*, edited by B. Piraux and K. Rzążewski (Kluwer Academic, Dordrecht, 2001), pp. 179–188.
[23] H. Z. Lu and A. D. Bandrauk, J. Chem. Phys. **115**, 1670 (2001).
[24] J. C. Light, I. P. Hamilton, and J. V. Lill, J. Chem. Phys. **82**, 1400 (1985).
[25] M. Hesse and D. Baye, J. Phys. B **32**, 5605 (1999).
[26] D. Baye, M. Hesse, J. M. Sparenberg, and M. Vincke, J. Phys. B **31**, 3439 (1998).
[27] J. T. Muckerman, R. V. Weaver, T. A. B. Kennedy, and T. Uzer, in *Numerical Grid Methods and Their Applications to Schrödinger's Equation*, edited by C. Cerjan (Kluwer Academic, Dordrecht, 1993), pp. 89–119.
[28] V. S. Melezhik and D. Baye, Phys. Rev. C **59**, 3232 (1999).
[29] K. Sakimoto, J. Phys. B **33**, 5165 (2000).
[30] D. Baye and P. H. Heenen, J. Phys. A **19**, 2041 (1986).
[31] E. S. Smyth, J. S. Parker, and K. T. Taylor, Comput. Phys. Commun. **114**, 1 (1998).
[32] W. E. Arnoldi, Q. Appl. Math. **9**, 17 (1951).
[33] R. Heather and H. Metiu, J. Chem. Phys. **86**, 5009 (1987).
[34] R. W. Heather, Comput. Phys. Commun. **63**, 446 (1991).
[35] S. Chelkowski and A. D. Bandrauk, Int. J. Quantum Chem. **30**, 473 (1996).
[36] S. Chelkowski, C. Foisy, and A. D. Bandrauk, Phys. Rev. A **57**, 1176 (1998).
[37] M. D. Feit and J. A. Fleck, J. Chem. Phys. **80**, 2578 (1983).

[38] H. Haken and H. C. Wolf, *Molecular Physics and Elements of Quantum Chemistry* (Springer-Verlag, Berlin, 1994).
[39] T. E. Sharp, At. Data **2**, 119 (1971).
[40] E. Cormier and P. Lambropoulos, J. Phys. B **29**, 1667 (1996).
[41] S. Vivirito, K. T. Taylor, and J. S. Parker, J. Phys. B **32**, 3015 (1999).
[42] J. S. Parker, E. S. Smyth, and K. T. Taylor, J. Phys. B **31**, L571 (1998).
[43] J. S. Parker, D. H. Glass, L. R. Moore, E. S. Smyth, K. T. Taylor, and P. G. Burke, J. Phys. B **33**, L239 (2000).
[44] D. Dundas, K. Meharg, J. F. McCann, and K. T. Taylor (unpublished).